Journal of Engineering Mathematics **38:** 119–140, 2000.

An Oseen-type model for swirling internal separated flows

K. SANJEEV RAO
Computational and Theoretical Fluid Dynamics Division, National Aerospace Laboratories, Bangalore 560 017, India

Received 3 June 1998; accepted in revised form 13 July 1999

Abstract. The viscous, laminar, separated flow downstream of a sudden expansion in a pipe is studied. The flow is modeled by an Oseen-type equation, but with the additional feature that the nonlinearity in the swirl is retained. Exact solutions are obtained for a high-Reynolds-number limit and for arbitrary Reynolds number by use of an eigenfunction-expansion procedure, in the presence of swirl. This leads to a non-standard eigenvalue problem. When the swirl is sufficiently large, a central recirculating region is observed. The effect of the pressure gradients on the velocity profiles and the central recirculating eddy is discussed. The low-Reynolds-number solutions go over smoothly to the large Reynolds number solution as the Reynolds number increases. Good agreement is obtained with the numerically computed value of the reattachment length.

Key words: Oseen model, swirl, internal separated flows, pipe flow, eigenvalues.

1. Introduction

The flow field of concern in this paper is sketched in Figure 1. Viscous, incompressible fluid enters an infinitely long circular pipe of radius R_1 by way of a sudden expansion from a symmetrically placed smaller pipe of radius R_0; the inlet flow, in general, is swirling. This is encountered under many situations, like for instance in combustion tubes, wind tunnels, physiological flows, etc. Let us assume that the inlet velocity profiles are given at the sudden expansion. Our interest then is in determining the flow downstream of the expansion, assumed to be steady and laminar, for all values of the Reynolds number, Re defined to be $W_m R_1/\nu$, where W_m is the value of the peak velocity of the Poiseuille flow far downstream.

The flow is governed by the Navier–Stokes (N–S) equations. One of the difficulties is, of course, that the N–S equations are nonlinear and we have no general method of solving such equations. A second difficulty is that, as the Reynolds number increases, the problems associated with two disparate length scales come into play. Third and most importantly, at

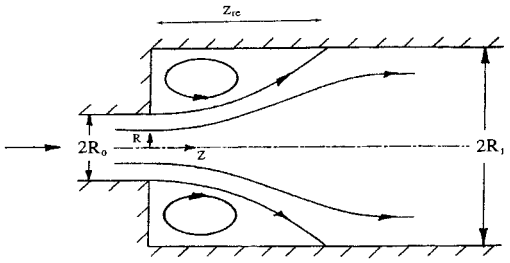

Figure 1. Sudden expansion in a pipe.

sufficiently high Reynolds numbers the flow is known to become turbulent; thus, although the inlet conditions may be steady, the flow downstream is unsteady with a behavior that *appears* to be random or chaotic in character. These difficulties explain why *simple* pipe flow is still an unsolved problem in fluid mechanics.

In this paper we model the steady, swirling laminar flow in the pipe, downstream of a sudden expansion, using equations in which the advection terms in the N–S equations have been linearized. We are partly motivated by the fact that there is still no method available to solve the full equations for all Reynolds numbers and partly by the fact that swirling flows are of considerable industrial importance (see for example [1, pp. 49–65] and [2, pp. 120–144]). Ramakrishnan and Shankar [3] showed in the plane case that model equations similar to the ones used here yield results that agree with those of the N–S equations at low Re and which show qualitative features very similar to those of the N–S equations for Re $\to \infty$. This Oseen approximation allows one to find analytical solutions in terms of an eigenfunction expansion over the whole range of Reynolds numbers. This feature is expected to carry over to the axisymmetric case, but with the additional and important possibility of dealing with swirl. We shall show that it is possible to retain a certain amount of nonlinearity pertaining to the swirl component which is crucial in the generation of central recirculating regions.

Before proceeding it may be worth indicating what exactly one could hope to find from the proposed model. Apart from determining the pressure-drop distribution in the pipe, one would hope to find the length of the wall-bounded recirculating regions downstream of the expansion and their dependence on the inlet swirl. One might also hope to find features entirely peculiar to the existence of swirl, for example *central* recirculating regions. The fact that all this can be attempted for the whole range of Re makes the model worthwhile in spite of its obvious limitations. The formulation of the present model is outlined in Section 2, solutions valid for Re $\to \infty$ are deduced in Section 3 while the solutions for arbitrary Re are obtained in Section 4.

2. Formulation

Let R be the radial coordinate, θ the azimuthal coordinate and Z the axial coordinate. Let the corresponding velocity components be U, V and W, respectively, and let P be the pressure. Note that all these quantities are dimensional. We normalize all lengths by the radius R_1 of the outer pipe, all velocities by the far downstream maximum velocity W_m of the Poiseuille flow, and pressure by ρW_m^2. Let u, v and w be the nondimensional velocity components and p the nondimensional pressure. The full, steady Navier–Stokes equations in nondimensional form are (Tritton [4, pp. 52]): (continuity)

$$u_r + \frac{u}{r} + \frac{v_\theta}{r} + w_z = 0, \tag{1a}$$

$$\left[uu_r + \frac{vu_\theta}{r} + wu_z - \frac{v^2}{r}\right] = -p_r + \frac{1}{\mathrm{Re}}\left[u_{rr} + \frac{u_r}{r} - \frac{u}{r^2} + \frac{u_{\theta\theta}}{r^2} + u_{zz} - \frac{2v_\theta}{r^2}\right], \tag{1b}$$

$$\left[uv_r + \frac{uv}{r} + \frac{vv_\theta}{r} + wv_z\right] = -\frac{p_\theta}{r} + \frac{1}{\mathrm{Re}}\left[v_{rr} + \frac{v_r}{r} - \frac{v}{r^2} + \frac{v_{\theta\theta}}{r^2} + v_{zz} + \frac{2u_\theta}{r^2}\right], \tag{1c}$$

$$\left[uw_r + \frac{vw_\theta}{r} + ww_z\right] = -p_z + \frac{1}{\mathrm{Re}}\left[w_{rr} + \frac{w_r}{r} + \frac{w_{\theta\theta}}{r^2} + w_{zz}\right], \tag{1d}$$

where the latter three represent axial, azimuthal and axial momentum, respectively. The subscripts denote the partial derivative with reference to that independent variable.

2.1. MODEL EQUATIONS

Far downstream, the radial and azimuthal components of the velocity vanish. The velocity is purely in the axial direction as $z \to \infty$, but its magnitude varies with the radius. The maximum value of this velocity is one, because of nondimensionalization. The present model that is linearized (except the nonlinear advection term in v) about the Poiseuille flow assumes that the flow is advected only by this unit axial velocity. The flow is assumed to be axisymmetric. Thus, the velocity components and pressure are assumed not to vary with θ. With this approximation, the radial momentum equation becomes.

$$u_z - \frac{v^2}{r} = -p_r + \frac{1}{\mathrm{Re}}\left(u_{rr} + \frac{u_r}{r} - \frac{u}{r^2} + u_{zz}\right). \tag{2a}$$

It is to be noted that the swirl velocity component v is still nonlinear in this equation. This gives rise to many interesting features.

The azimuthal momentum equation is

$$v_z = \frac{1}{\mathrm{Re}}\left(v_{rr} + \frac{v_r}{r} - \frac{v}{r^2} + v_{zz}\right). \tag{2b}$$

The axial momentum equation becomes

$$w_z = -p_z + \frac{1}{\mathrm{Re}}\left(w_{rr} + \frac{w_r}{r} + w_{zz}\right). \tag{2c}$$

It may be noted that the inertial terms are still present in these equations in a modified form that simplifies the equations considerably. Since the flow goes to Poiseuille flow far downstream, the approximations are clearly reasonable there. However, one cannot easily justify these in the neighborhood of the sudden expansion. In fact, the z-advection term even has the wrong sign over part of the separated flow region near the walls, but here the heads are very small and this may not matter much. For the plane case Ramakrishnan and Shankar [3] obtained interesting results that were at least qualitatively correct and in a similar fashion our results appear to show these approximations to be useful. We are able to abtain a physically realistic velocity field in simple analytical form over the whole range of Reynolds numbers $0 < \mathrm{Re} < \infty$. We believe this provides some justification for the kind of quasi-linearization that we have used.

The pressure term in Equations (2a) and (2c) can be eliminated by cross-differentiation and subtraction. There is an axisymmetric stream function ψ such that

$$w = \frac{\psi_r}{r}, u = -\frac{\psi_z}{r}. \tag{3}$$

On substituting this in Equation (2), we get

$$\left(L - \mathrm{Re}\frac{\partial}{\partial z}\right) L\psi = 2\,\mathrm{Re}\, v v_z, \tag{4}$$

where

$$L = \frac{\partial^2}{\partial r^2} - \frac{1\partial}{r\partial r} + \frac{\partial^2}{\partial z^2}. \tag{5}$$

Thus, in summary, Equations (2b) and (4) constitute the model that we shall be employing to describe approximately the swirling flow downstream of a sudden expansion in a pipe. The model is Oseen-like in that the acceleration terms are approximated by uniform advection in the axial direction. However, some effect of nonlinearity is retained, with significant effect, through the swirl term in the radial momentum equation. As far as the boundary conditions are concerned, we assume that there is no slip on the side walls, and that the velocity field takes on the values prescribed initially at $z = 0$; far downstream the field has to develop into the appropriate Poiseuille flow.

2.2. SWIRL COMPONENT

The swirl component of the velocity v satisfies Equation (2b), which is second order in z. This equation reveals that the azimuthal velocity component completely decouples from the other two. On assuming a solution of the form $v(r, z) = \hat{v}(r)\,\mathrm{e}^{-lz}$, we get

$$(r\hat{v}_r)_r - \frac{\hat{v}}{r} + (l^2 + l\,\mathrm{Re})r\hat{v} = 0. \tag{6}$$

The hat denotes that the relevant quantity varies only with r and not with z.

The solution for the swirl is [4] $\hat{v} = J_1(\sqrt{l^2 + l\,\mathrm{Re}}\,r)$ where $J_n(r)$ is the Bessel function of the first kind of order n. Clearly, $\hat{v}$ vanishes at the wall, *i.e.* at $r = 1$. Hence $J_1(\sqrt{l^2 + l\,\mathrm{Re}}) = 0$. The function $J_1(r)$ has infinitely many zeros, denoted here by δ_n. As a result, l also can take infinitely many possible values. They are denoted by l_n. We have $\sqrt{l_n^2 + l_n\,\mathrm{Re}} = \delta_n$. The full swirl as a function of both r and z is given by

$$v(r, z) = \sum_{n=1}^{\infty} K s_n J_1(\delta_n r)\,\mathrm{e}^{-l_n z}, \tag{7}$$

where K is the amplitude of the inlet swirl and s_n is the n^{th} expansion coefficient. At $z = 0$, the nondimensional swirl has an inlet profile $v_0(r)$. It is here taken to be

$$v_0(r) = K(r^3 - 2r_0 r^2 + r_0^2 r), \tag{8}$$

where r_0 is the inlet radius. It is generally taken to be 0·5 unless specified otherwise. For this inlet swirl profile, the swirl number can be computed from the expression (see, for example Sloan *et al.* [5])

$$S = \int_{r_1}^{r_2} r^2 v_0(r) w_0(r)\,\mathrm{d}r \Big/ \left(r_2 \int_{r_1}^{r_2} r w_0^2(r)\,\mathrm{d}r \right). \tag{9}$$

A swirl amplitude of one roughly corresponds to a swirl number of five. The exact ratio is 5·02232143.

Experiments [5] show that the swirl initially has a solid body rotation character, reaches a maximum and then decreases in some manner. For the inlet swirl profile taken here, the

linear term dominates at small r. After the maximum, the decay is taken to be polynomial for simplicity.

It can be shown that the expansion coefficients can be evaluated from the expression

$$s_n = 2\int_0^{r_0} r v_0(r) J_1(\delta_n r)\,\mathrm{d}r \Big/ (K(J_0(\delta_n))^2). \tag{10}$$

In general, the larger the number of terms in the expansion (10), the smaller is the maximum error in satisfying the inlet profile. But this decrease in error is not monotonic.

3. An approximation for large Reynolds number

The general model equation that has been proposed here is quasi-linear. Even in the plane case, in the absence of swirl, where the equations are linear, Ramakrishnan and Shankar [3] found that the solution leads to a nontrivial, nonstandard eigenvalue problem. Naturally, we should expect the swirling flow considered here to lead to an even more complicated situation. It is shown in [3] that there is a very natural, 'boundary-layer'-like approximation that could be applied for $\mathrm{Re} \to \infty$. We expect a similar approximation to be valid in our case too. Moreover, this analysis provides the basis functions in terms of which the general solutions can be expanded. Hence, we will discuss this limiting case before considering the general situation.

3.1. No swirl

The length scale along r is assumed to be of order unity and that along z is assumed to be the Reynolds number Re. The functions ψ and w are assumed to be of order one, and u to be of order 1/Re, and to leading order, the governing equations become

$$\left(L_1 - \mathrm{Re}\frac{\partial}{\partial z}\right) L_1\psi = 2\,\mathrm{Re}\, v v_z, \tag{11}$$

where the operator L_1 is

$$L_1 = \frac{\partial^2}{\partial r^2} - \frac{1}{r}\frac{\partial}{\partial r}.$$

On assuming a solution of the form $\psi = \mathrm{e}^{-\lambda z}\phi(r)$, we have the eigenvalue problem

$$(L_1 + \lambda\,\mathrm{Re})L_1\phi = L_1(L_1 + \lambda\,\mathrm{Re})\phi = 0, \quad \phi(1) = \phi'(1) = 0 \tag{12}$$

with the solution

$$\phi_n = r^2 - \frac{r J_1(\sqrt{\lambda_n\,\mathrm{Re}}\,r)}{J_1(\sqrt{\lambda_n\,\mathrm{Re}})}, \tag{13}$$

where the λ's satisfy the eigenvalue condition

$$\frac{\sqrt{\lambda\,\mathrm{Re}}\,J_0(\sqrt{\lambda\,\mathrm{Re}})}{J_1(\sqrt{\lambda\,\mathrm{Re}})} = 2. \tag{14}$$

At these eigenvalues are real, like in the plane case of [3].

Sufficiently far downstream, the stream function $\hat{\psi}$ should become that for Poiseuille flow:

$$\hat{\psi}_\infty(r) = \mathrm{c}r^2(2 - r^2). \tag{15a}$$

Here, c is determined by the volumetric flow at the inlet.

The eigenfunctions given by Equation (13) form a complete set. Hence, at other points, the general stream function as a function of r and z can be expanded in terms of these functions. Using the property of linear superposition of the stream function, we have

$$\psi(r, z) = \hat{\psi}_\infty(r) + \sum_{n=1}^{\infty} a_n \phi_n(r)\, \mathrm{e}^{-\lambda_n z}, \tag{15b}$$

where $\lambda_n = \alpha_n^2/\mathrm{Re}$ and $\phi_n(r) = r^2 - r J_1(\alpha_n r)/J_1(\alpha_n)$.

At the inlet, the stream function is assumed to correspond to a parabolic axial velocity profile that vanishes for $r_0 \leqslant r \leqslant 1$. Hence

$$\hat{\psi}_0(r, r_0) = c\left(\frac{r}{r_0}\right)^2\left(2 - \left(\frac{r}{r_0}\right)^2\right), \qquad 0 \leqslant r \leqslant r_0. \tag{15c}$$

It follows from mass conservation that the c in this expression is the same as that which appears in $\hat{\psi}_\infty(r)$.

The inlet condition should be applied strictly at a distance that is sufficiently far and upstream to the expansion. But at large Reynolds number, the upstream influence is negligible. Smith [6, 7] shows that the upstream influence becomes considerable only for very small Reynolds numbers. Hence the inlet condition is applied just before the expansion.

The eigenfunctions, given by Equation (13) are orthogonal. This can be used to get an expression in closed form for the coefficients. We have

$$a_n = \frac{-2\displaystyle\int_0^1 (\psi_0(r) - \psi_\infty(r)) J_1(\alpha_n r)\, \mathrm{d}r}{J_1(\alpha_n)}. \tag{16}$$

The coefficients can also be computed by the constraint that the error in satisfying the inlet condition by minimized. This is the 'Least Squares Procedure' that is discussed in Ramakrishnan and Shankar [3]. This gives coefficients that agree very well with those given by Equation (16), as can be seen in Table II.

We computed the inlet stream function by taking twenty-five terms in the expansion given by Equation (15b). It is seen that this agrees very well with the exact stream function given by Equation (15c). Computations show that, as more and more terms are taken in the expansion, the maximum error in satisfying the inlet profile decreases monotonically.

Plots of the lines of constant axisymmetric stream function are very similar to those of the plane duct of Ramakrishnan and Shankar [3].

The limiting streamline that separates from the top corner of the inlet reattaches at a point on the outer pipe (Figure 1). The axial distance from the inlet to this point is called the reattachment (recirculation) length. The flow inside the recirculating region is very weak.

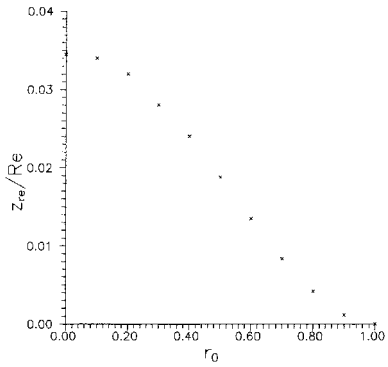

Figure 2. Variation of the corner reattachment length with inlet radius as $\mathrm{Re} \to \infty$, $K = 0$.

This is a dead water region, and the corner recirculation is not seen. This does not happen at finite Reynolds number, as will be seen in Subsection 4.1.

Figure 2 shows that the corner reattachment length decreases as the inlet radius r_0 increases. These values are almost the same as that in Figure 3 of Ramakrishnan and Shankar [3]. The smaller the value of r_0, the larger is the reattachment length. This is also observed in the experiments of Chaturvedi [8], Back and Roschke [9] and Abujelala and Lilley [10], and the computation of Chang *et al*. [11].

3.2. Swirling flows at large Reynolds number ($\mathrm{Re} \to \infty$)

The governing equation when swirl is present is now

$$\left(L_1 - \mathrm{Re}\frac{\partial}{\partial z}\right) L_1\psi = 2\,\mathrm{Re}\, v v_z, \tag{17}$$

where

$$L_1 = \frac{\partial^2}{\partial r^2} - \frac{1}{r}\frac{\partial}{\partial r}.$$

By using linear superposition, the total streamfunction is broken up into two parts, one that does not depend on swirl, and another which does. The former was solved and discussed in the previous sub-section. The streamfunction that is solved in Equation (17) is the latter one.

On substituting the expression for the swirl, given by Equation (7), in Equation (17), we get

$$\left(L_1 - \mathrm{Re}\frac{\partial}{\partial z}\right) L_1\psi = -2\sum_{m=1}^{\infty}\sum_{n=1}^{\infty} K^2\delta_n^2 s_m s_n J_1(\delta_m r) J_1(\delta_n r)\, \mathrm{e}^{-(\delta_m^2+\delta_n^2)z/\mathrm{Re}}. \tag{18}$$

Let

$$\psi = \sum_{m=1}^{\infty}\sum_{n=1}^{\infty} h_{mn}(r) \exp\left(-\frac{\delta_{mn}^2 z}{\mathrm{Re}}\right), \tag{19a}$$

where

$$\delta_{mn}^2 = \delta_m^2 + \delta_n^2. \tag{19b}$$

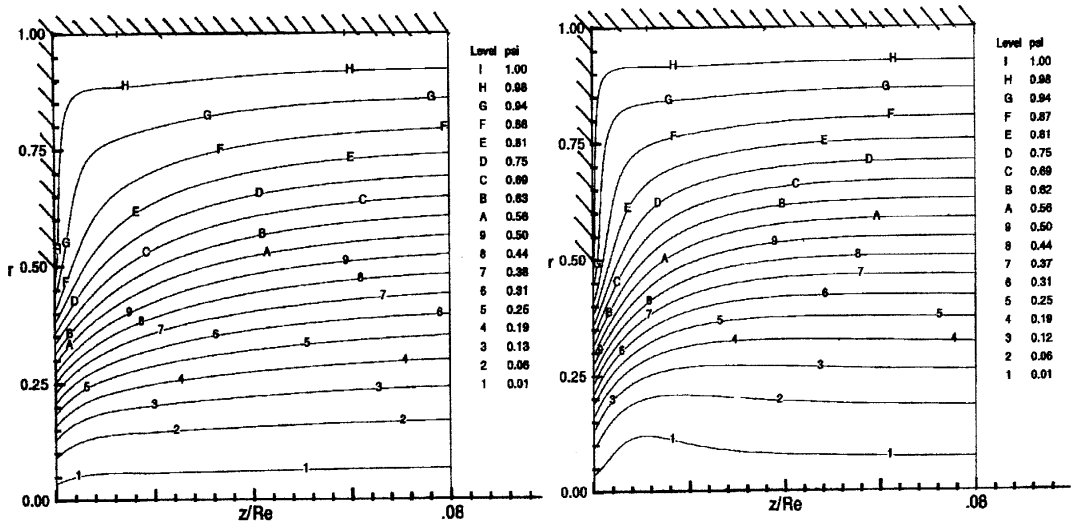

a. $K = 2{\cdot}00$ b. $K = 2{\cdot}67$

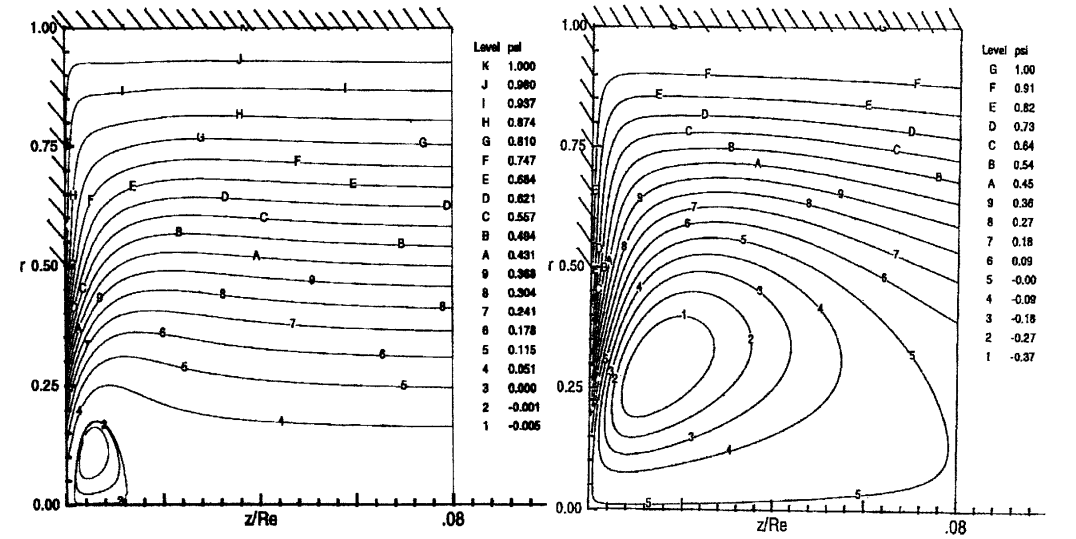

c. $K = 3{\cdot}00$ d. $K = 5{\cdot}00$

Figure 3. Lines of constant axisymmetric streamfunction, Expansion ratio = 2, Re $\rightarrow \infty$.

Equations (18) and (19) imply

$$\left(\frac{\mathrm{d}^2}{\mathrm{d}r^2} - \frac{1}{r}\frac{\mathrm{d}}{\mathrm{d}r} + \delta_{mn}^2\right)\left(\frac{\mathrm{d}^2}{\mathrm{d}r^2} - \frac{1}{r}\frac{\mathrm{d}}{\mathrm{d}r}\right) h_{mn} = -2K^2 s_m s_n \delta_n^2 J_1(\delta_m r) J_1(\delta_n r) \tag{20}$$

for each m and n. This is a fourth-order inhomogeneous differential equation. The solutions to the homogeneous part of this equation can be shown to be $w_1(r) = d$ where d is a constant, $w_2(r) = r^2$, $w_3(r) = rJ_1(\delta_{mn}r)$ and $w_4(r) = rY_1(\delta_{mn}r)$. The particular solution to the inhomogeneous Equation (20) is obtained by the method of variation of parameters (Dettman [12, pp. 300–301]), in terms of these four solutions. The final expression for the total stream function is

$$\psi(r, z) = \hat{\psi}_\infty(r) + \sum_{m=1}^{\infty}\sum_{n=1}^{\infty} h_{mn}(r) \exp\left(-\frac{\delta_{mn}^2 z}{\mathrm{Re}}\right) + \sum_{k=1}^{\infty} a_k \phi_k(r) \exp\left(-\frac{\alpha_k^2 z}{\mathrm{Re}}\right), \tag{21}$$

where

$$h_{mn}(r) = c_1(r) + (c_2(r) + b_{mn})r^2 + (c_3(r) + c_{mn})rJ_1(\delta_{mn}r) + c_4(r)rY_1(\delta_{mn}r),$$

$$c_1 = -K^2 \int_0^r \frac{t_1(r)}{D(r)}[w_2(w_3''w_4' - w_3'w_4'') + w_3(w_2'w_4'' - w_2''w_4') + w_4(w_2''w_3' - w_2'w_3'')]\,\mathrm{d}r,$$

$$c_2 = K^2 \int_0^r \frac{t_1(r)}{D(r)}(w_3''w_4' - w_3'w_4'')\,\mathrm{d}r \qquad c_3 = K^2 \int_0^r \frac{t_1(r)}{D(r)}(w_2'w_4 - w_2w_4')\,\mathrm{d}r$$

$$c_4 = K^2 \int_0^r \frac{t_1(r)}{D(r)}(w_2''w_3' - w_3w_2')\,\mathrm{d}r \qquad t_1(r) = -2K^2 s_m s_n \delta_n^2 J_1(\delta_m r) J_1(\delta_n r)$$

$$D(r) = w_4'''(w_2''w_3' - w_2'w_3'') - w_3'''(w_2''w_4' - w_2'w_4'').$$

Side-wall boundary conditions determine the constants b_{mn} and c_{mn}. Equation (16), which gives an expression for the coefficients, gets modified to

$$a_k = \frac{-2}{J_1(\alpha_k)} \int_0^1 [\psi_0(r, r_0) - \hat{\psi}_\infty(r) - \sum_{m=1}^{\infty}\sum_{n=1}^{\infty} h_{mn}(r)]J_1(\alpha_k r)\,\mathrm{d}r. \tag{22}$$

It is interesting to note that the full stream function depends only on the square of the swirl amplitude K^2, and not on K.

Figures 3(a) to 3(d) show the two-dimensional steamline plots of swirling flows, *i.e.* lines of constant axi-symmetric streamfunction ψ, when K is 2·0, 2·67, 3·0 and 5·0, respectively. Although inlet swirl does modify the sudden expansion flow, for example by affecting the reattachment length and causing downstream swirl, at relatively small amplitudes the qualitative features remain the same, as seen in Figure 3(a). However, when the inlet swirl amplitude is comparatively large, a qualitatively new feature appears, *i.e.* a central recirculation region. When the inlet swirl amplitude is 2·0, there is no central recirculation. When the amplitude is increased to 2·67, computations show that, over an interval of z sufficiently close to the axis the axial velocities are negative. Hence, there is an onset of central recirculation, even though it is not big enough to be seen in the figure. It becomes visible when the swirl amplitude is

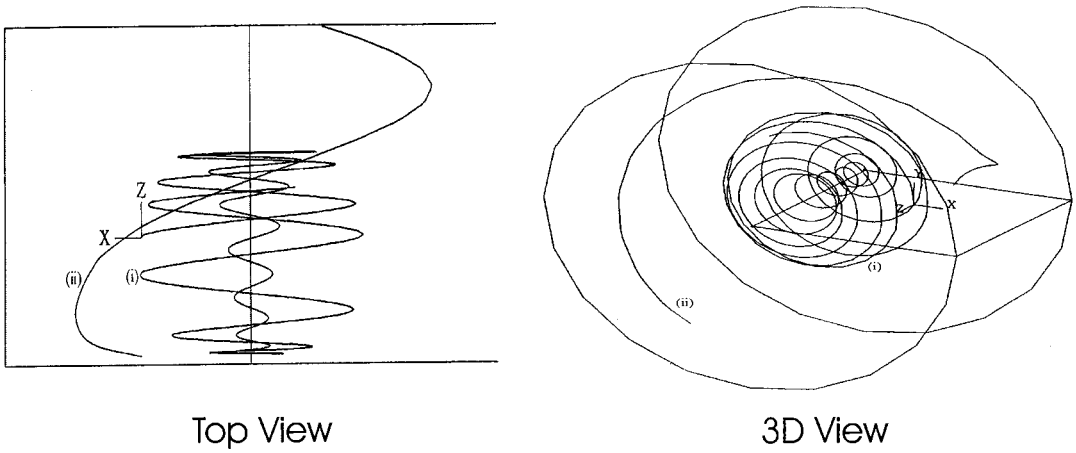

Figure 4. Three dimensional streamlines following two particles plotted using CFD view. $K = 5{\cdot}0$. (i) particle inside the central recirculation region; (ii) particle outside the central recirculation region.

increased further. It is also seen that the central recirculation grows progressively as the swirl amplitude is increased. These figures are qualitatively very similar to those of Ahmed [13]. In these figures, the corner recirculation that is expected (because of sudden expansion) is squeezed close to the side wall, as the axial length is normalized by the Reynolds number Re, like the case where there was no swirl.

If the nonlinear v^2 term is dropped in the radial momentum Equation (2a), the radial and azimuthal momentum equations decouple. The resulting system is similar to the $v = 0$ case, where there is no central recirculation. Hence, it is this nonlinear term that brings in interesting features. Some idea of the richness of this flow can be obtained by looking at the three-dimensional plots.

Figures 4(a) and 4(b) show the three-dimensional streamlines that we plotted using the commercial software CFD View. These are obtained by tracking particles released at various positions. Figure 4(a) shows that, when the particle is inside the central recirculation zone (trajectory i), it moves on the inside of the torus and comes back on the outer surface. It is to be noted that the trajectory does not return on itself. Thus, the motion on the torus can be in closed or open orbits, though on a finite-precision machine, only closed orbits are seen, however large the closing period may be. When the particle is initially outside the recirculation region (trajectory ii), it goes out of the z interval. Figure 4(b) shows a three-dimensional view of this picture. The inner and outer regions of the torus are seen very clearly. When the integration is done for a larger period, the trajectories fill out the torus more and more.

Figures 5(a) and 5(b) show certain quantitative predictions that the model makes about the effect of swirl. Figure 5(a) shows that the corner reattachment length decreases with increase in the swirl. It is interesting to note that, when the swirl amplitude is 0·64, this decrease is very steep. An increase in the swirl amplitude squeezes the corner recirculation region. Hence this effect is understandable. This also agrees qualitatively with the observation of Abujelala and Lilley [10].

If the critical swirl is defined as a dimensionless swirl at which the central eddy first appears, Figure 5(b) shows that this decreases with increasing inlet radius r_0. For a

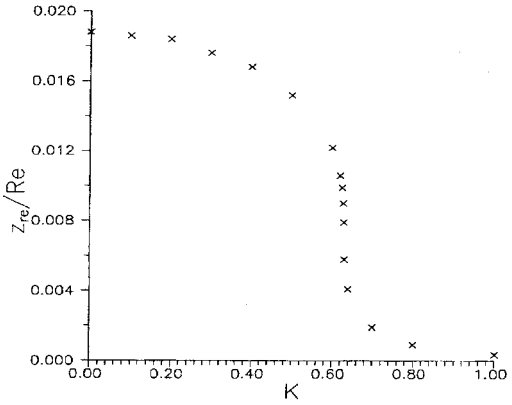

Figure 5(a). Variation of the corner reattachment length with swirl amplitude as Re $\to \infty$, $r_0 = 0{\cdot}5$.

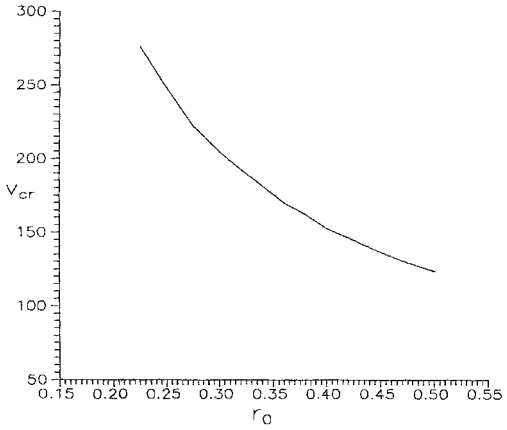

Figure 5(b). Variation of critical non-dimensional swirl with inlet radius as Re $\to \infty$.

given far-stream velocity, decreasing the inlet radius r_0 increase the inlet axial velocity. The inlet swirl has to be comparable with the inlet axial velocity for the central eddy to be seen. Hence, the critical swirl varies inversely with the inlet radius.

Calculations show that the pressure field is strongly dependent on the strength of the inlet swirl. As was already pointed out above, when $K > 2{\cdot}67$, a central recalculation bubble exists very close to the entry. It may therefore be of some interest to examine the axial pressure gradient as a function of z at given radial locations. This is done in Figure 6 for $r = 0{\cdot}05$ and $0{\cdot}8$. Note that in both figures Re $\partial p/\partial z$ is plotted against z/Re for four values of the swirl amplitude K.

The central recirculation bubble is incipient at $K \approx 2{\cdot}67$ when the expansion ratio is two. Figure 6(a) shows exactly the pressure gradient that we would expect in the flow near the axis of the pipe in the absence of swirl. The flow is expanding to fill the pipe and as a consequence the fluid near the axis suffers a continuous deceleration. As a consequence, the pressure gradient is positive, decreasing, till far downstream where ultimately it takes on the negative value determined by the Poiseuille flow there. When $K = 1$, the situation is somewhat different, with a much more rapid decay of the pressure gradient to a minimum, followed by an increase and then a more gradual decay to the ultimate value. For $K = 2$ and 3 the situation is similar, except that the minimum is now negative and, consequently, there is an increase to the ultimate asymptotic value. It is of some importance to note that when $K = 3$, the interval $0{\cdot}0002 < z/\mathrm{Re} < 0{\cdot}012$ actually lies inside the recirculation bubble. We will point out the importance of this later, after we have considered the velocity profiles. Note that the range in this figure was restricted to $z/\mathrm{Re} < 0{\cdot}04$ since we wished here to emphasize the field inside the bubble. As regards $r = 0{\cdot}8$, we only wish to point out that the profile in (a) is connected with the corner recirculation, which is absent for $K \geqslant 1$.

We now consider the distribution of the axial velocity component $w(r, z)$ close to the sudden expansion. In Figures 7(a)–7(c), this component is plotted as a function of r at five z-stations for three different values of the inlet swirl. When $K = 2$ we observe a pattern in the profiles that only gets intensified as K increases. Even when z/Re is as small as $0{\cdot}001$, the velocity profile shows a dip on the axis indicating a deceleration there. Note that with our normalization w is always 4 on the axis at $z = 0$. As z increases we note that, for r less than

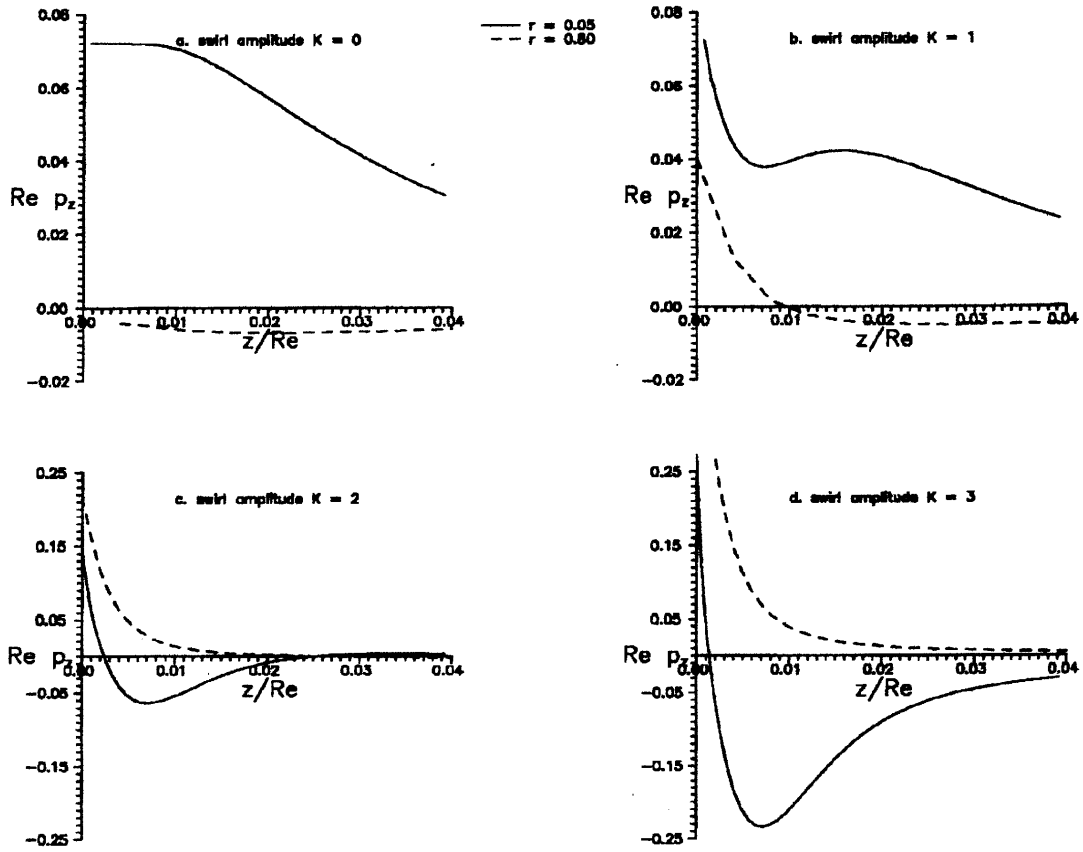

Figure 6. Variation of axial pressure gradient with z at $r = 0{\cdot}05$ & $0{\cdot}8$ as $\mathrm{Re} \to \infty$, $r_0 = 0{\cdot}5$.

an approximate value of 0·4, there is a deceleration of the flow which is most pronounced at the axis, while for $r > 0{\cdot}4$ there is an acceleration of the flow. Although this cannot be seen from the figure, note that for sufficiently large z the profiles get gradually transformed to the Poiseuille form, with a maximum unit velocity on the axis and a monotonic decay to zero on the wall. The profiles, it may also be observed, are normal at the axis, as indeed they must be.

In Figure 7(b) the profiles shown are for a swirl amplitude of 2·67. This is the approximate value at which the central recirculation bubble is incipient. The profiles are very similar to those shown in Figure 7(a), except for one crucial difference: now the velocity on the axis is less than one for $z/\mathrm{Re} > 0{\cdot}002$. In fact, at a particular axial station the velocity goes to zero. Of course, beyond this the fluid near the core has to accelerate to its asymptotic value of 1. Thus, the fluid near the core initially suffers a deceleration and then undergoes an acceleration to its final value for downstream. We can now guess what will happen when K is increased further to 3, (Figure 7(c)). Now the initial deceleration at the axis continues until the velocity on the axis is actually negative before accelerating to its final value.

The most interesting feature of these swirling flows is, without doubt, the formation of a central recirculation bubble when the swirl amplitude is sufficiently high, just like the observation of vortex breakdown in confined geometries when the swirl exceeds a critical value, as in Suematsu *et al.* [14], Uchida *et al.* [15], Eshudier [16], Delery [17], Shtern and Hussain [18], among others. While we connot claim to be able to give a fully self-contained explanation for

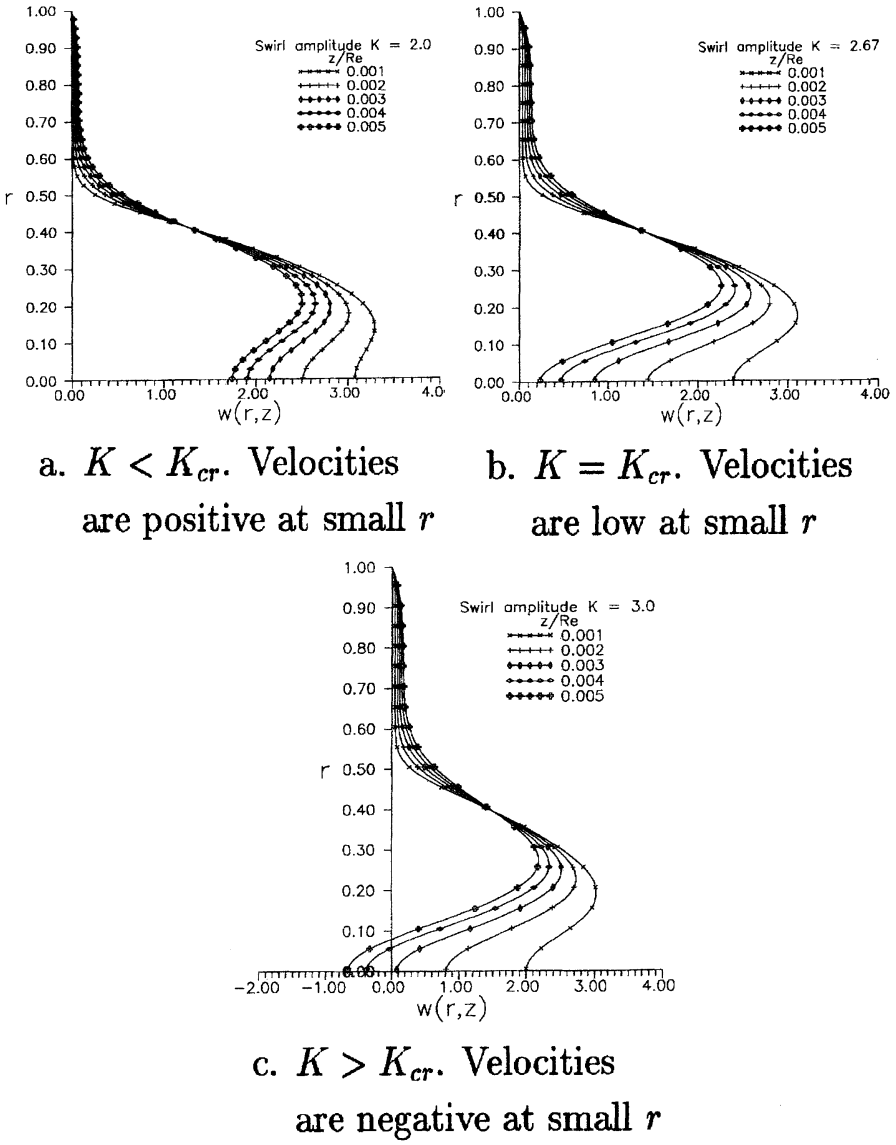

a. $K < K_{cr}$. Velocities are positive at small r

b. $K = K_{cr}$. Velocities are low at small r

c. $K > K_{cr}$. Velocities are negative at small r

Figure 7. Axial velocity profiles as a function of r at different z stations as $\mathrm{Re} \to \infty$, $r_0 = 0{\cdot}5$.

this phenomenon, the axial velocity profiles and pressure gradients discussed earlier suggest a reason for the existence of these special eddy structures and their nature. Figures 7(a)–7(c) clearly show that with swirl the fluid near the pipe axis suffers a deceleration which increases with increased swirl amplitude. This deceleration is over and above the central deceleration in a swirlless flow that is necessary to account for the fluid that is being entrained by the high-speed inlet flow.

Two important facts are to be noted:

(a) the increased central deceleration with K,

(b) the absence of any significant deceleration for $r \approx 0{\cdot}4$.

Now recall the radial momentum Equation (2a). For a fixed large Reynolds number, as K increases the dominant terms in the equation will be the centripetal term and the radial pressure gradient over a significant portion of the pipe, away from the axis and not too close to the wall. In other words, this implies that the pressure field will be determined primarily by the swirl velocity. Since the swirl velocity decays very little (at high Reynolds numbers) near the inlet, this also implies that the axial pressure gradient in these regions, which are swirl-dominated, is negligible. We can then argue from the z-momentum equation that there is little axial deceleration in these layers. In other words, with increased swirl, some layers of fluid away from the axis will, on account of their 'swirling inertia', travel downstream with little deceleration. But, while this happens, the layers near the wall still have to be accelerated, by viscous shear. Since now the middle regions do not decelerate as explained above, the core region where there is little swirl now has to decelerate more than before. With increased K, the contribution from the core increases, until negative velocities are reached and the bubble is formed. This is by no means a full explanation, but it appears that this does at least explain why central deceleration is necessary with increased K. This is also seen in Brown and Lopez [19] for axisymmetric flows, where it is shown that the centripetal force due to the swirl that balances the radial pressure gradient leads to an adverse pressure gradient near the axis. Computations reveal that the azimuthal component of vorticity becomes negative on the axis for $0{\cdot}002 < z/\mathrm{Re}\, 0{\cdot}012$ during the onset of central recirculation.

The central recirculation is seen only at large Reynolds numbers (in the presence of sufficiently large swirl) and not at small Reynolds numbers, as will be noted in Section 4. Hence, this is primarily an inviscid phenomenon. Nevertheless, the pressure profiles in Figure 6 tell us something important about the role of viscosity in the dynamics of the recirculating region. This is best seen from Figure 6d, for the case $K = 3$. Here the bubble lies approximately in the region $0{\cdot}002 < z/\mathrm{Re} < 0{\cdot}012$. It will be observed that in this interval the pressure gradient is negative throughout. But, at this radial station, the axial velocity in the bubble, from Figure 3c, starts out positive, goes to zero and then remains negative all the way to the other side (downstream side) of the bubble boundary. This means that $\partial w/\partial z$ is negative over at least a portion of the bubble. Since the pressure gradient is negative throughout, this implies that the viscous terms must play a role in the dynamics of the bubble, even at high Reynolds numbers.

4. Solutions for arbitrary Reynolds number

The purpose of this paper is to formulate a model that works at *all* Reynolds numbers, and goes smoothly to the limiting form discussed in the previous section. Hence, the general case, valid for arbitrary values of the Reynolds number, will be taken up.

4.1. No swirl

The governing equation here is

$$\left(L - \mathrm{Re}\frac{\partial}{\partial z}\right) L\psi = 0, \quad L = \frac{\partial^2}{\partial r^2} - \frac{1}{r}\frac{\partial}{\partial r} + \frac{\partial^2}{\partial z^2}. \tag{23}$$

When this is compared with the previous case, where the Reynolds number was large, there is an additional term $\partial^2/\partial z^2$ in the linear operator L. Hence, this is a second-order equation

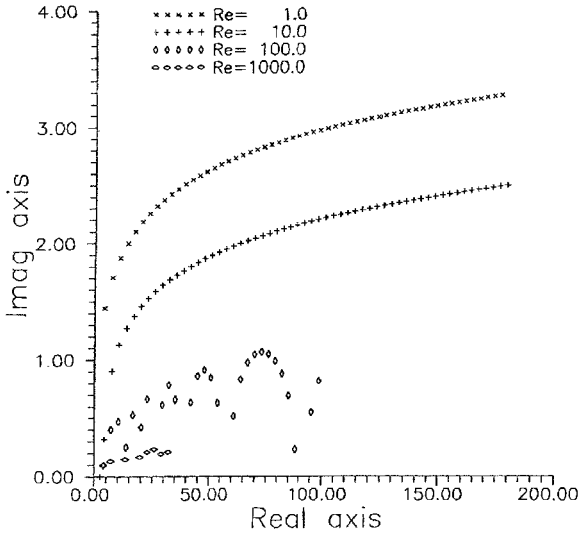

Figure 8. Distribution of eigenvalues in the first quadrant of the complex plane.

in z. Two conditions will have to be specified at the inlet. One of these is the axial velocity, as before. In additional, the radial velocity profile is also specified. It is taken to be identically zero at the inlet.

A solution of the form $\psi(r, z) = \phi(r)\, \mathrm{e}^{-\beta z}$ is substituted in Equation (23). The eigenvalue β appears in a nonlinear manner here. This implies that it is complex in general. The expressions $rJ_1(\beta r)$ and $rJ_1(\sqrt{\beta^2 + \beta\,\mathrm{Re}}\, r)$ are obtained as the solutions of the two second-order partial differential equations. The wall boundary conditions imply that the eigenvalues satisfy the condition

$$\frac{J_1(\beta)}{\beta J_0(\beta)} = \frac{J_1(\sqrt{\beta^2 + \beta\,\mathrm{Re}})}{\sqrt{\beta^2 + \beta\,\mathrm{Re}}\, J_0(\sqrt{\beta^2 + \beta\,\mathrm{Re}})}. \tag{24}$$

If β is an eigenvalue, $-\beta$ and β^* are also eigenvalues. The additional physical constraint of the boundedness of solutions restricts the relevant eigenvalues to be only in the first quadrant of the complex plane. As in the plane case discussed in Ramakrishnan and Shankar [3], there is an upper bound to the imaginary part of an eigenvalue with a given real part. This can be verified by the principle of an argument [12, pp. 211–213].

The eigenvalues of the plane case, given in Ramakrishnan and Shankar [3], act as good starting values to compute the present ones. They are refined by a Newton–Raphson procedure as before. To check that no eigenvalues are missed, the principle of the argument is used to find the total number of eigenvalues within a given region in the right half of the complex plane.

Figure 8 shows the distribution of eigenvalues for $\mathrm{Re} = 1$, 10, 100 and 1000. At $\mathrm{Re} = 1$ all eigenvalues are complex. When the real parts of these eigenvalues are sufficiently large, the eigenvalues are equally spaced. Both the real and imaginary part keep increasing monotonically. The same is true when $\mathrm{Re} = 10$, except that the first eigenvalue is real. But at $\mathrm{Re} = 100$ the pattern is different. There is some sort of oscillation, and the amplitude appears to become bigger when the real part increases. As the Reynolds number Re increases, more and more real eigenvalues are found. They tend to crowd near the origin. But even around 90 there are real

eigenvalues. No order is apparent in their distribution. At Re = 1000, the complex eigenvalues have lesser order. Table I shows the first twenty-five eigenvalues (ordered according to the real part) when Re is 1, 10, 100 and 1000

The eigenfunctions are given by

$$\phi_k(r) = r J_1(\beta_k r) - \frac{J_1(\beta_k) r J_1(\sqrt{\beta_k^2 + \beta_k \operatorname{Re}} r)}{J_1(\sqrt{\beta_k^2 + \beta_k \operatorname{Re}})}. \tag{25}$$

At a finite Reynolds number Re, both real and complex eigenvalues are found in general. Let there be N_r real eigenvalues α_k with real eigenfunctions $\phi_k(r)$ and N_i complex eigenvalues β_k with complex eigenfunctions $\chi_k(r)$. By superposition the full axisymmetric stream function is given by

$$\psi(r, z) = \hat{\psi}_\infty(r) + \sum_{k=1}^{N_r} a_k \phi_k(r)\, \mathrm{e}^{-\alpha_k z} + \mathfrak{Re}\left(\sum_{k=1}^{Ni} b_k \chi_k(r)\, \mathrm{e}^{-\beta_k z} \right). \tag{26}$$

The coefficients a_k and b_k are determined by the constraint that at the expansion $z = 0$, the inlet streamfunction $\hat{\psi}_0(r)$ is reproduced, and the radial velocity profile is identically zero. Unlike in the previous section, these complex eigenfunctions are not orthogonal. Hence the method of least squares has to be used to find the coefficients.

Figure 9(a) shows the lines of constant axi-symmetric streamfunction when the Reynolds number Re is 1. Unlike the case where the Reynolds number was large, the corner recirculation region can be resolved very well. Except near the expansion, all the streamlines are almost parallel.

4.2. Swirling flows at arbitrary Reynolds number

Here the governing equation is

$$\left(L - \operatorname{Re} \frac{\partial}{\partial z} \right) L\psi = 2 \operatorname{Re} v v_z. \tag{27}$$

After substituting Equation (7) for the swirl, we get the right-hand side of Equation (27) to be

$$-2 \operatorname{Re} K^2 \sum_{m=1}^{\infty} \sum_{n=1}^{\infty} s_m s_n l_n J_1(\alpha_m r) J_1(\alpha_n r)\, \mathrm{e}^{-(l_m + l_n) z},$$

where $l_n = (-\operatorname{Re} + \sqrt{\operatorname{Re}^2 + 4\delta_n^2})/2$. Let $l_{mn} = l_m + l_n$. On assuming a solution of the form

$$\psi = \sum_{m=1}^{\infty} \sum_{m=1}^{\infty} H_{mn}(r)\, \mathrm{e}^{-l_{mn} z} \tag{28}$$

and substituting this in Equation (27), we get

$$\sum_{m=1}^{\infty} \sum_{n=1}^{\infty} \left(\frac{\mathrm{d}^2}{\mathrm{d}r^2} - \frac{1}{r} \frac{\mathrm{d}}{\mathrm{d}r} + l_{mn}^2 + l_{mn} \operatorname{Re} \right) \left(\frac{\mathrm{d}^2}{\mathrm{d}r^2} - \frac{1}{r} \frac{\mathrm{d}}{\mathrm{d}r} + l_{mn}^2 \right) H_{mn}\, \mathrm{e}^{-l_{mn} z}$$

$$= -2 \operatorname{Re} K^2 \sum_{m=1}^{\infty} \sum_{n=1}^{\infty} s_m s_n l_n J_1(\alpha_n r) J_1(\alpha_m r)\, \mathrm{e}^{-l_{mn} z}. \tag{29}$$

Table 1. The first 25 eigenvalues for Re = 1, 10, 100 and 1000.

k	Re = 1			Re = 10			Re = 100			Re = 1000		
1	4·231	+	1·444i	2·470			4·012	+	0·097i	0·003		
2	4·231	−	1·444i	4·277	+	0·317i	4·012	−	0·097i	0·007		
3	7·453	+	1·706i	4·277	−	0·317i	5·626			0·135		
4	7·453	−	1·706i	7·322	+	0·903i	7·022	+	0·397i	0·219		
5	10·631	+	1·874i	7·322	−	0·903i	7·022	−	0·397i	0·322		
6	10·631	−	1·874i	10·390	+	1·128i	8·636			0·446		
7	13·794	+	1·999i	10·390	−	1·128i	10·232	+	0·464i	0·589		
8	13·794	−	1·999i	13·480	+	1·271i	10·232	−	0·464i	0·752		
9	16·950	+	2·099i	13·480	−	1·271i	12·250			0·934		
10	16·950	−	2·099i	16·583	+	1·375i	13·622	+	0·249i	1·136		
11	20·102	+	2·182i	16·583	−	1·375i	13·622	−	0·249i	1·358		
12	20·102	−	2·182i	19·695	+	1·458i	16·291	+	0·524i	1·600		
13	23·251	+	2·254i	19·695	−	1·458i	16·291	−	0·524i	1·861		
14	23·251	−	2·254i	22·813	+	1·528i	18·210			2·142		
15	26·398	+	2·316i	22·813	−	1·528i	19·918	+	0·419i	2·443		
16	26·398	−	2·316i	25·936	+	1·587i	19·918	−	0·419i	2·764		
17	29·545	+	2·371i	25·936	−	1·587i	22·675	+	0·665i	3·106		
18	29·545	−	2·371i	29·063	+	1·639i	22·675	−	0·665i	3·476		
19	32·690	+	2·421i	29·063	−	1·639i	25·432			3·832i	+	0·095
20	32·690	−	2·421i	32·192	+	1·686i	25·521			3·832i	−	0·095
21	35·836	+	2·467i	32·192	−	1·686i	27·137			4·210		
22	35·836	−	2·467i	35·323	+	1·728i	29·320	+	0·614i	4·638		
23	38·980	+	2·508i	53·323	−	1·728i	29·320	−	0·614i	5·078		
24	38·980	−	2·508i	38·455	+	1·767i	32·165	+	0·781i	5·537		
25	42·124	+	2·547i	38·455	−	1·767i	32·165	−	0·781i	6·017		

Consider now a particular component of m and n. The solutions of the homogeneous equation are $W_1 = rJ_1(l_{mn}r)$, $W_2 = rY_1(l_{mn}r)$, $W_3 = rJ_1(k_{mn}r)$ and $W_4 = rY_1(k_{mn}r)$ where $k_{mn} = \sqrt{l_{mn}(l_{mn} + \mathrm{Re})}$. The solution of the inhomogeneous equation is again obtained by the method of variation of parameters. The expression for the full streamfunction is

$$\psi(r,z) = \hat{\psi}_\infty(r) + \sum_{m=1}^{\infty}\sum_{n=1}^{\infty} H_{mn}(r)\,\mathrm{e}^{-l_{mn}z} + \sum_{k=1}^{N_r} a_k\phi_k(r)\,\mathrm{e}^{-\alpha_k z} + \mathfrak{Re}\left(\sum_{k=1}^{N_i} b_k\chi_k(r)\,\mathrm{e}^{-\beta_k z}\right), \tag{30}$$

where

$$H_{mm}(r) = (C_1(r) + B_{mn})W_1(r) + C_2(r)W_2(r) + (C_3(r) + C_{mn})W_3(r) + C_4(r)W_4(r),$$

$$C_1(r) = K^2\int_0^r \frac{D_1T_1(r)\,\mathrm{d}r}{\mathrm{Den}(r)}, \qquad C_2(r) = K^2\int_0^r \frac{D_2T_1(r)\,\mathrm{d}r}{\mathrm{Den}(r)},$$

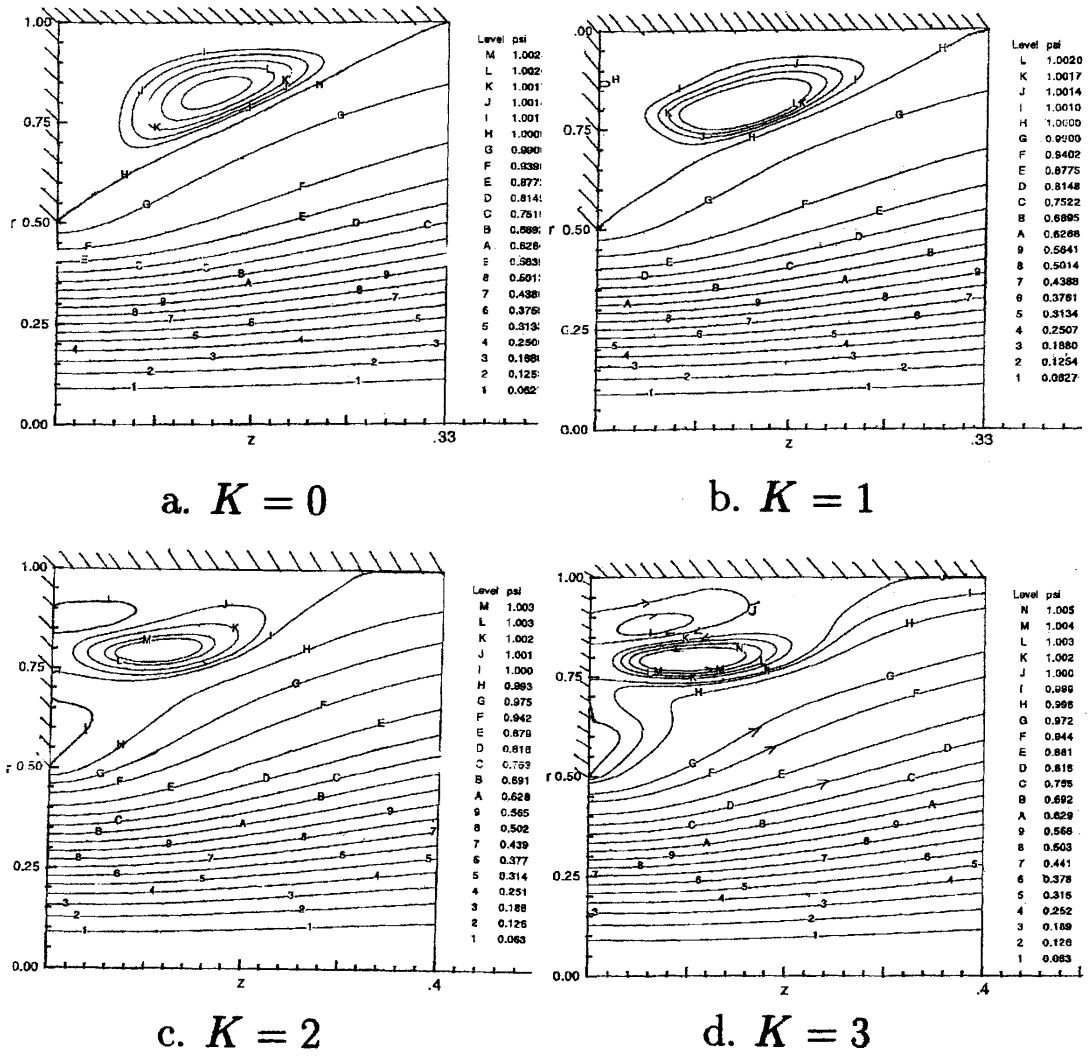

Figure 9. Lines of constant axisymmetric streamfunction Expansion ratio = 2, Re = 1·0.

$$C_3(r) = K^2 \int_0^r \frac{D_3 T_1(r)\,\mathrm{d}r}{\mathrm{Den}(r)}, \qquad C_2(r) = K^4 \int_0^r \frac{D_4 T_1(r)\,\mathrm{d}r}{\mathrm{Den}(r)},$$

$$T_1(r) = -2\,\mathrm{Re}\,K^2 \sum_{m=1}^{\infty}\sum_{n=1}^{\infty} s_m s_n l_n J_1(\alpha_n r) J_1(\alpha_m r)\,\mathrm{e}^{-l_{mn} z},$$

$$\mathrm{Den}(r) = D_1 W_1''' - D_2 W_2''' + D_3 W_3''' - D_4 W_4''',$$

$$D_1 = \begin{vmatrix} W_2 & W_3 & W_4 \\ W_2' & W_3' & W_4' \\ W_2'' & W_3'' & W_4'' \end{vmatrix}, \quad D_2 = \begin{vmatrix} W_1 & W_3 & W_4 \\ W_1' & W_3' & W_4' \\ W_1'' & W_3'' & W_4'' \end{vmatrix},$$

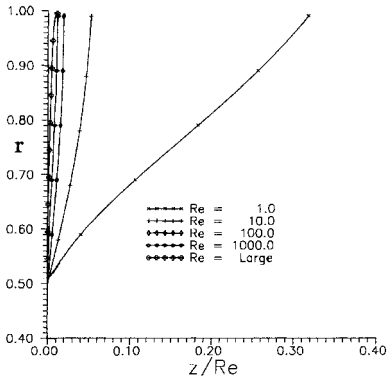

Figure 10. Limiting streamline for various Re. No Swirl, $r_0 = 0{\cdot}5$.

$$D_3 = \begin{vmatrix} W_1 & W_2 & W_4 \\ W_1' & W_2' & W_4' \\ W_1'' & W_2'' & W_4'' \end{vmatrix}, \quad D_4 = \begin{vmatrix} W_1 & W_2 & W_3 \\ W_1' & W_2' & W_3' \\ W_1'' & W_2'' & W_3'' \end{vmatrix}.$$

The constants B_{mn} and C_{mn} are determined by the side-wall boundary conditions, as before.

For small swirl the flow is qualitatively very similar to the plane case. When the swirl amplitude is increased to 1 at Re $= 1$, an additional recirculation region begins to appear at the corner, as seen in Figure 9(b). This is similar to the experimental observation of Durrett *et al*. [20]. Figure 9(c) shows that, when the swirl amplitude is made 2, this additional recirculation region becomes bigger. Figure 9(d) resolves the structure of this inner recirculation region when the swirl amplitude is made 3. Increasing the swirl tends to enlarge these secondary regions and intensify them. Moffatt [21] showed that, in general, there will be an infinite number of corner eddies of diminishing size and intensity. There is no corresponding theorem in the axisymmetric or three-dimensional case (even though Liu and Joseph [22] present Stokes flow toroidal vortices in a conical trench), but by analogy one would expect a similar result to hold. But it is hard to say whether these are related to the Moffatt eddies or whether they are due to swirl alone.

Figure 10 shows that as the Reynolds number Re increases, the limiting streamline ($\psi = 1$) converges uniformly to the high-Re result. As Re increases, more and more coefficients become real. The coefficients themselves converge to that of the high-Re approximation. These results show that the high-Re approximation is valid.

Figure 11(a) shows that at sufficiently large Re, in the absence of swirl, z_{re}/Re reaches an asymptotic limit of 0·0188. This implies that the increase of z_{re} with Re at sufficiently large Re is linear. This agrees with the observations of Back and Roschke [9] and Abujelala and Lilley [10] for the axisymmetric case. It may be noted that Ramakrishnan and Shankar [3] also get the same result for the planar case. However, Dennis and Smith [23] find that the increase in the corner reattachment length with Re is logarithmic for the flow through a two-dimensional symmetric constriction. For comparison, the reattachment lengths have also been computed using a Navier–Stokes code (see, for example, Majumdar *et al*. [24]). Figure 11(b) shows the analytical and the computed values for a top-hat inlet profile of the axial velocity. Very good agreement is seen, even at a Reynolds number of 1000. Computation of the reattachment lengths for a parabolic inlet profile of the axial velocity is not available. But, it is seen that the

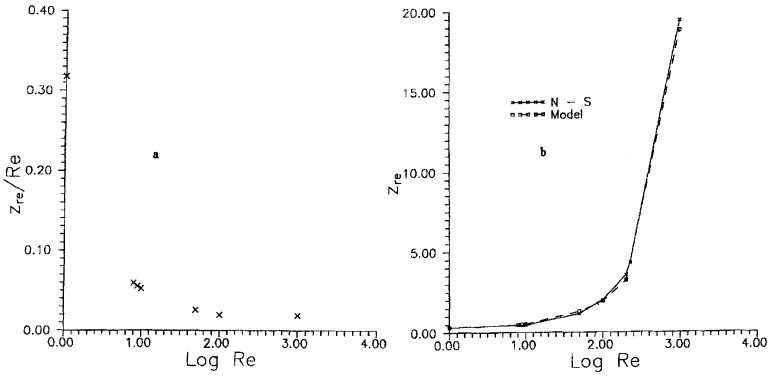

Figure 11. Variation of corner reattachment length with Re, No Swirl, $r_0 = 0{\cdot}5$.

analytical values of the reattachment lengths for the parabolic and top-hat inlet profiles of the axial velocity do not differ much.

The notion of comparing the results of our model with those found in experiments should be placed in proper perspective. The present model is a linearized version of the steady Navier–Stokes equations and the solutions found are intrinsically laminar in nature. Most of the experimental results that are referred to deal with turbulent flows, whose mixing properties are so different from those of laminar flows that we cannot expect to find anything more than qualitative similarity. This cannot be helped; one could, alternatively, refrain from dealing with the experimental data altogether; but this would lead one to lose the insights that can be gained from them. A comparison that would be entirely meaningful is one with the results of laminar calculations based on the full, steady Navier–Stokes equations. This was done with reasonable success in the plane case by Ramakrishnan and Shankar [3]. They consider Hung and Macagno [25] who use a numerical finite-difference method and are limited in Reynolds number, and Kumar and Yajnik [26] who derive a boundary-layer-like limit equation for high Reynolds numbers. However, we have not found such calculations for the swirling flows considered here.

5. Conclusion

The principal result of this paper has been the suggestion of a quasi-linear model for laminar, swirling, internal separated flows that can be solved exactly for all Reynolds numbers. This is useful, as the Navier–Stokes equations themselves are intractable analytically, except for $\mathrm{Re} \to 0$, even for the simple geometry considered here. In fact, as far as we know, there is no other model that works even qualitatively over the whole range of Reynolds numbers. The model no doubt has its limitations, the principal one being the restriction to laminar flows. All real flows are turbulent at sufficiently high Reynolds numbers and so the model, which presumably approximates the possible laminar solutions of the Navier–Stokes equations, can at best reproduce only the qualitative features of real flows. It should also be pointed out that the quasi-linearization of the convective terms, in the spirit of the Oseen equations, makes the model inaccurate in the near field close to the sudden expansion. It may be surprising that, in spite of all these obvious limitations, the model yields fields that display many of the important features of swirling internal separated flows.

Even though the present model is Oseen like, there are differences too:

Table 2. The first 25 coefficients for the representation of the inlet stream-function, obtained by least squares procedure and by the use of orthogonality. $K = 0, r_0 = 0{\cdot}5, \mathrm{Re} \to \infty$.

n	a_n	a_n	n	a_n	a_n
	Least squares	Orthogonality		Least squares	Orthogonality
1	6·33018E-05	6·33016E-05	14	−8.21667E-08	−8.15338E-08
2	−1·21821E-05	−1·21822E-05	15	−3·26059E-08	−3·37946E-08
3	−3·53354E-06	−3·53384E-06	16	5·62444E-08	5·71284E-08
4	2·38513E-06	2·38504E-06	17	2·24561E-08	2·09732E-08
5	8·27043E-05	8·26653E-07	18	−4·01762E-08	−3·89590E-08
6	−8·40242E-07	−8·40232E-07	19	−1·61155E-08	−1·79966E-08
7	−3·10649E-07	−3·11143E-07	20	2·96906E-08	3·13698E-08
8	3·88698E-07	3·88822E-07	21	1·19529E-08	9·46782E-09
9	1·48348E-07	1·47726E-07	22	−2·25587E-08	−2·01331E-08
10	−2·10751E-07	−2·10487E-07	23	−9·10836E-09	−1·27134E-08
11	−8·19429E-08	−8·27174E-08	24	1·75401E-08	2·15300E-08
12	1·26826E-07	1·27254E-07	25	7·09899E-09	−3·13418E-10
13	4·99087E-08	4·89482E-08			

- Far downstream, the Poiseuille flow has a velocity that varies with r. The actual flow is advected by this non-uniform velocity, but it is implicit assumption of this model that this can be looked upon as being advected by a unit axial velocity. It is interesting to note that, in spite of this assumption, the model predicts the qualitative features of the actual flow.
- The swirl component of the velocity introduces nonlinearity into this model. This gives rise to many interesting features. It is seen that, when there is no swirl, the three momentum equations are completely linear, and the axi-symmetric problem is similar to the plane case, where there is no central recirculation (Ramakrishnan and Shankar [3]). Hence, it is the swirl that brings in the possibility of central recirculation, which is a ubiquitous feature in vortex breakdown, combustors, etc. This sheds light on the importance of swirl in understanding these complex phenomena.

Acknowledgement

The author thanks Dr. P. N. Shankar for suggesting this problem, for useful discussions and help in preparing this manuscript. The generosity of Dr. Sekhar Majumdar in lending his Navier–Stokes solver and the help rendered by Ms. B. N. Rajani in running it are acknowledged.

References

1. A. K. Gupta, D. G. Lilley and N. Syred, *Swirl Flows*. Kent: Abacus Press (1984) 475pp.
2. J. M. Beer and N. A. Chigier, *Combustion Aerodynamic*. London: Applied Science Publishers (1972) 264pp.
3. S. V. Ramakrishnan and P. N. Shankar, The Oseen model for internal separated flows. *J. Enging. Math.* 16 (1982) 325–347.

4. D. J. Tritton, *Physical Fluid Dynamics*. London: Van Nostrand Reinhold (1980) 362pp.
5. D. G. Sloan, P. J. Smith and L. D. Smoot, Modelling of swirl in turbulent flow systems. *Prog. Energy Combust. Sci.* 12 (1986) 163–250.
6. F. T. Smith, Flow through constricted or dilated pipes and channels: Part 1. *Q. J. Mech. Appl. Math.* 29 (1976) 343–364.
7. F. T. Smith, Flow through constricted or dilated pipes and channels: Part 2. *Q. J. Mech. Appl. Math.* 29 (1976) 365–376.
8. M. C. Chaturvedi, Flow characteristics of axi-symmetric expansions. *ASCE J. Hydraulics Div.* 89 (1963) 61–92.
9. L. H. Back and E. J. Roschke, Shear layer regimes, wave instabilities and reattachment lengths downstream of an abrupt circular channel expansion. *J. Appl. Mech. Trans. A.S.M.E* 94 (1972) 677–681.
10. M. T. Abujelala and D. G. Lilley, Swirl confinement and nozzle effects on confined turbulent flow. AIAA Paper 84–1377 (1984).
11. K. C. Chang, H. C. Soong and C. I. Uang, Examination of numerical skills for flows in sudden expansion type combustors. *Fourth Asian Cong. Fluid Mech.*, Hong Kong, Paper (1989) F125–128.
12. J. W. Dettman, *Applied Complex Variables*. New York: Macmillan (1965) 481pp.
13. S. A. Ahmed, Turbulent velocity characteristics of different swirlers in a model combustor. *Sixth Asian Cong. Fluid Mech.*, Singapore, Paper (1995) 1384–1387.
14. Y. Suematsu, T. Ito and T. Hayase, Vortex breakdown phenomenon in a circular pipe. *Bull. JSME* 29 (1986) 2086–2094.
15. S. Uchida, Y. Nakamura and M. Ohsawa, Experiments on the axi-symmetric vortex breakdown in a swirling air flow. *Trans. J. Soc. Aero. Space Sci.* 27 (1985) 206–216.
16. M. P. Escudier, Vortex breakdown: Observations and explanations. *Prog. Aero. Sci.* 25 (1988) 189–229.
17. J. M. Delery, Aspects of vortex breakdown. *Prog. Aero. Sci.* 30 (1994) 1–59.
18. V. N. Shtern and F. Hussain, Collapse, Symmetry Breaking and Hysteresis in Swirling Flows. *Ann. Rev. Fluid Mech.* 31 (1999) 537–566.
19. G. L. Brown and J. M. Lopez, Axi-symmetric vortex breakdown: Part 2. Physical mechanisms. *J. Fluid Mech.* 221 (1990) 553–576.
20. R. P. Durrett, W. H. Stevenson and H. D. Thompson, Radial and axial turbulent flow measurements with an LDV in an axi-symmetric sudden expansion air flow. *ASME J. Fluids Eng.* 110 (1988) 367–372.
21. H. K. Moffatt, Viscous and resistive eddies near a sharp corner. *J. Fluid Mech.* 18 (1964) 1–18.
22. C. H. Lui and D. D. Joseph, Stokes flow in conical trenches. *SIAM J. Appl. Math.* 34 (1978) 286pp.
23. S. C. R. Dennis and F. T. Smith, Steady flow through a channel with a symmetrical constriction in the form of a step. *Proc. R. Soc. London A* 372 (1980) 393–414.
24. S. Majumdar, B. N. Rajani and N. Ansari, *Numerical Prediction of Turbulent Flow Around Axi-Symmetric Underwater Bodies Using a Pressure Based Finite Volume Algorithm*. Second Asian CFD Conf., Tokyo, Paper (1986) 451–456.
25. T. K. Hung and E. O. Macagno, Laminar eddies in a two-dimensional conduit expansion. *La Houille Blanche* 21 (1966) 391–401.
26. A. Kumar and K. S. Yajnik, Internal separated flows at large Reynolds number. *J. Fluid Mech.* 97 (1980) 27–51.